Understanding and Embracing the Complexities of the Molecular Communication Channel in Liquids

Jiaming Wang, Dongyin Hu, Chirag Shetty, Haitham Hassanieh
University of Illinois at Urbana-Champaign
{jw27, dyhu, cshetty2, haitham}@illinois.edu

ABSTRACT

Molecular communication has recently gained a lot of interest due to its potential to enable micro-implants to communicate by releasing molecules into the bloodstream. In this paper, we aim to explore the molecular communication channel through theoretical and empirical modeling in order to achieve a better understanding of its characteristics, which tend to be more complex in practice than traditional wireless and wired channels. Our study reveals two key new characteristics that have been overlooked by past work. Specifically, the molecular communication channel exhibits non-causal inter-symbol-interference and a long delay spread, that extends beyond the channel coherence time, which limit decoding performance. To address this, we design, μ-Link a molecular communication protocol and decoder that accounts for these new insights. We build a testbed to experimentally validate our findings and show that μ-Link can improve the achievable data rates with significantly lower bit error rates.

CCS CONCEPTS

• **Networks → Cyber-physical networks**; *Physical links.*

KEYWORDS

Molecular Communication, Diffusion, Non-Causal Channel, Micro-Implants, Inter-Symbol-Interference, Viterbi.

ACM Reference Format:
Jiaming Wang, Dongyin Hu, Chirag Shetty, Haitham Hassanieh. 2020. Understanding and Embracing the Complexities of the Molecular Communication Channel in Liquids. In *The 26th Annual International Conference on Mobile Computing and Networking (MobiCom '20), September 21–25, 2020, London, United Kingdom.* ACM, New York, NY, USA, 15 pages. https://doi.org/10.1145/3372224.3419191

MobiCom '20, September 21–25, 2020, London, United Kingdom

ACM ISBN 978-1-4503-7085-1/20/09…$15.00
https://doi.org/10.1145/3372224.3419191

1 INTRODUCTION

Molecular communication (MC) has emerged as a promising technology for communication through fluids such as micro-implants communicating through the bloodstream or sensors communicating through industrial pipes [4, 20, 34]. In MC, a device can transmit data by releasing molecules into the fluid which are then transported and detected at a receiver [55]. For example, a device can release molecules to encode a "1" bit and release nothing to encode a "0" bit. The receiver can measure the concentration of molecules to determine whether the transmitted bit was a "1" or a "0".

Molecular communication has the potential to enable micro and nano-implants to communicate with each other inside the human body and coordinate sensing and actuation tasks. Recent advances in biomedical sciences have in fact led to the development of nano-implants that can sense human vitals from inside the body and even travel through the bloodstream to perform targeted drug delivery and treatment [12, 30, 55]. There is significant interest in enhancing the operation of such implants by connecting them using MC [4, 5, 9, 10, 20–23, 34, 53]. MC presents a suitable alternative to other communication technologies such as wireless. In particular, RF signals do not propagate well in fluids and form factor constraints prevent scaling RF radios to micro and nano-dimensions [40, 56, 66]. In contrast, for MC, researchers can design synthetic cells that send and receive molecular signals [17, 52, 57], nano-scale Lab-on-a-Chip that monitor chemical content [30, 54, 61], and bio-implants that collect and process data [41, 43, 51].

While there is still a long way to realize the above vision, this paper takes steps to achieve a better understanding of the characteristics of the MC channel from both theoretical and empirical perspectives. The MC channel tends to be more complex in practice than standard RF, optical, or copper wire channels [28]. Understanding and addressing the differences between these channels and MC allows us to improve the performance of molecular communication.

There has been a significant amount of work on theoretically modeling the MC channel [15, 16, 46, 47, 47, 58, 59, 62, 65, 68]. However, these models tend to be overly simplified with assumptions that do not hold in practice (e.g. no inter-symbol-interference) or overly fitted to a closed form

equation that does not capture practical constraints and imperfections (see section 7 for more details). Hence, these models are only evaluated through simulations. On the other hand, there has been little work on empirically validating the MC channel models in fluids [19, 24, 60]. Performance in these testbeds yields at best a data rate of 4 bits/sec with 3% bit error rate (BER) [18]. However, this is achieved by using deep neural networks to decode MC signals without explicitly learning or modeling the channel. While promising, the approach requires the network to be trained for the specific channels being tested and hence, might not generalize to new channels that the neural network has not seen before as we show in section 6.

In this paper, we build on the above theoretical and empirical work to capture the characteristics of the MC channel.We introduce two new key properties that have been overlooked by past work on MC. Specifically, the molecular communication channel exhibits non-causal inter-symbol-interference and a long delay spread that extends beyond the channel coherence time. We show how to leverage these new insights to improve the decoding performance and achieve a higher bit rate with lower bit errors. We also empirically validate and incorporate insights introduced by past work such as the presence of signal dependent noise and the channel response resulting from the statistical behavior of molecular diffusion.

Our work, in particular, reveals the following two insights:

- **Non-causal Inter-Symbol-Interference:** Due to the statistical nature of diffusion, molecules released at the transmitter can arrive at significantly different times at the receiver even if they follow the same path. As a result, the molecules of previous symbols can arrive late creating inter-symbol-interference (ISI). Molecules of future symbols can arrive earlier than molecules of the current symbol creating a non-causal ISI as well. In contrast, in standard communication systems, ISI is caused only by previously transmitted symbols which can be decoded first to eliminate their ISI as opposed to future unknown symbols that cannot be decoded before the current symbol.
- **Long Delay Spread vs. Coherence Time:**[1] In MC channels, the channel delay spread can be long (1 to 4 seconds) which is of a similar order to the channel coherence time (a few 10s of seconds) [3, 26]. Hence, the channel varies only slightly slower than the time it takes us to estimate it. Compare this to RF channels where the delay spread ($0.1\mu s - 10\mu s$) is orders of magnitude smaller than the coherence time ($10ms - 100ms$) and we can quickly estimate the channel and assume to be constant for the duration of packet transmission. However, in MC, simply estimating the channel impulse response and using it to decode the bits throughout the packet leads to poor performance.

[1]Coherence time refers to the time for which the channel impulse response can be considered as static. Delay spread refers to the length of the channel impulse response, i.e., the time between the start and end of particles corresponding to the same symbol arriving at a receiver.

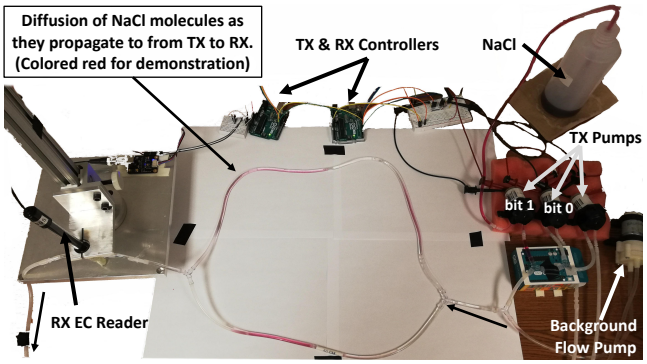

Figure 1: Experimental testbed for molecular communication in fluids. The testbed consists of a background pump that generates a bulk flow of water, pumps that transmit a "1" bit by releasing NaCl (Salt) or "0" bit by releasing water. The salt solution is dyed red to show its diffusion through the tube. The receiver is an EC meter that measures the conductivity which is proportional to the concentration of salt in the fluid.

To address the above issues, we design μ-Link a molecular communication protocol and decoder. Due to non-causal ISI, μ-Link cannot sequentially decode bits. Instead, it jointly decodes the current, future, and past symbols. To do so, the receiver first estimates the channel impulse response using known preamble bits transmitted at the beginning of the packet. This allows it to know how many past and future symbols will interfere with the current symbol being decoded. We then design a sliding window block Viterbi decoder that jointly decodes bits by accounting for both future and past symbols. The decoder, however, suffers from high complexity. To address this, we incrementally build the decoding graph starting from the preamble and accounting only for valid transitions and the k highest probability states where k is a tunable parameter. As a result, we can maintain linear-time decoding with negligible degradation in performance.

The above μ-Link decoder, however, works under the assumption that the channel impulse response is static. As discussed earlier, the channel changes in the same order as the time it takes us to estimate the channel. Hence, constantly re-estimating the channel will result in a huge overhead that leads to a very low data rate. To address this, we modify the Viterbi decoder to jointly decode the bits and concurrently update the estimation of the channel. Specifically, the decoder uses the soft values of the decoded bits as a confidence metric to decide which bits were correctly decoded. The correctly decoded bits are then used to update the estimate of the channel which is then used to improve the decoding.

We validate our MC channel model and the performance of our μ-Link decoder using an MC experimental testbed.

The testbed follows a similar approach to past experimental testbeds on validating the molecular communication channel [19, 60]. Our testbed is shown in Fig. 1. It consists of a network of narrow tubes and a pump that maintains a constant flow of water in the tubes. Another pump is used as a transmitter to release salt particles in the flowing liquid and a sensor is used as the receiver to measure the presence and concentration of these particles (See section 5 for more details). Our results confirm the MC channel characteristics we highlighted and show that by addressing these characteristics, we can improve the data rate and reduce the bit errors to achieve $5-10$ bits/sec with $0.2\%-5\%$ BER. This is $2.5\times$ the data rate for the same BER or $20\times$ lower BER for the same data rate as compared to [19] without the need to train and use neural networks which suffer from overfitting as we show in the results.

Contributions: The paper has the following contributions:

- It highlights two new key characteristics of the MC channel. To the best of our knowledge, none of the past work address these two characteristics which significantly limits the achievable data rates in practice.
- It presents a system that accounts for the characteristics of the MC channel and specifically addresses the issues of non-causality and long delay spread.
- It experimentally validates the findings and demonstrates improvement in achievable data rates and BER.

2 BACKGROUND

In this section, we present a primer on molecular communication in fluids. For further background, we refer the reader to section 7 as well as the following surveys [4, 20, 34].

MC is a communication paradigm inspired by chemical signaling between cells such as neurotransmitters and stimulating hormones. Similar to how neurotransmitters release molecules to signal an adjacent neuron, a device can transmit data by releasing molecules into the medium which are detected at a nearby receiver. While MC can work in both gaseous and liquid mediums, this paper focuses on MC in fluids due to its potential biomedical applications for communication between micro and nano-implants. In particular, we assume the device releases molecules into a flowing liquid in a micro-tube as shown in Fig. 1.[2]

A. MC Transmitter: The transmitter can encode data bits by adjusting the amount of released molecules, the type of released molecules, or both [2, 8]. The simplest form of encoding is OOK (On-OFF Keying) where releasing molecules represents a "1" bit and not releasing molecules represents a "0" bit. Since the aim of this paper is to understand the characteristics of the MC channel, we adopt an OOK encoding. OOK helps simplify our analysis of the channel and is likely to be the most practical type of encoding for future applications like micro-implants.

B. MC Receiver: The receiver can decode the transmitted bits by measuring the number of released molecules in the liquid. In theory, there are two types of receivers: destructive (active) or non-destructive (passive). Non-destructive receivers simply use a sensor to measure the concentration of molecules and decode the bits [36]. The molecules are then eliminated through the bulk flow of the liquid. Destructive receivers, on the other hand, absorb the molecules from the medium in order to decode the bits [14, 18]. In this paper, we focus on non-destructive receivers since they are simpler to implement using sensors making them more practical for MC applications. We also assume the receiver response is linear, i.e., the measured value at the receiver is linearly related to the concentration/number of molecules at the receiver.

C. MC Channel: The transmitted molecules are transported from the transmitter to the receiver through molecular propagation which is governed by three physical properties: *advection*, *molecular diffusion*, and *turbulent diffusion* [28].

- *Advection* refers to the transport of molecules along a bulk flow. For example, in biomedical applications, this could be the flow of the blood stream that carries molecules from one location to another. Advection significantly speeds up the delivery of molecules which from a communication perspective reduces the latency of communication.
- *Molecular Diffusion* refers to the random motion of molecules as they collide with neighboring substances in the medium and spread throughout the space. Molecular diffusion is inevitable in nature since particles are self-propelled by thermal energy which results in a well-known phenomenon called *Brownian Motion*.
- *Turbulent Diffusion* refers to the random motion of molecules due to mass transport. It occurs much more rapidly than molecular diffusion and is characterized by chaotic changes in pressure and flow velocity. It is well common in nature such as in blood flow or air flow.

The above properties is formally described using *Fick's Law* and the *advection-diffusion* equation which describe the statistical behavior of large amount of molecules [38]:

$$\frac{\partial C}{\partial t} + \nabla \cdot (\vec{\mathbf{v}} C) = \nabla \cdot (D \nabla C) + R \tag{1}$$

In the above equation, $C(\vec{\mathbf{x}}, t)$ denotes the concentration of particles as a function of location $\vec{\mathbf{x}}$ and time t; $\vec{\mathbf{v}}$ denotes the velocity vector (v_x, v_y, v_z) of the advection bulk flow; ∇C denotes the gradient of C and $\nabla\cdot$ denotes the divergence of

[2]Note that, in a gaseous medium like air, wireless RF is a far superior mode of communication as compared to MC. Hence, we focus on MC in fluids since RF signals do not propagate well in fluids.

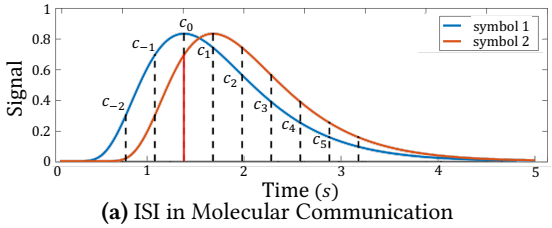

(a) ISI in Molecular Communication

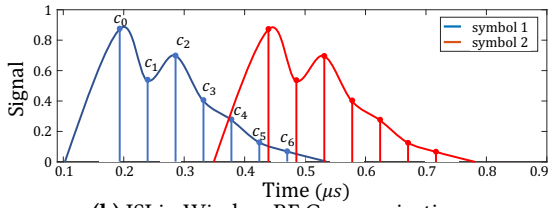

(b) ISI in Wireless RF Communication

Figure 2: Intern-Symbol-Interference (ISI) in MC vs. RF channels.

the vector. $R(\vec{\mathbf{x}}, t)$ represents the input molecules released by the transmitter at a given location and time. Finally, D denotes the diffusion coefficient. Note that *Fick's Law* applies to both molecular and turbulent diffusion with a different values of D.[3] Since the value of D is typically much larger for turbulent diffusion, it is common to ignore molecular diffusion in presence of turbulence [1].

For simplicity, we assume a 1D unbounded channel since we focus on MC in micro-tubes. The transmitter is at the origin $\vec{x_t} = \vec{0}$ and releases an impulse of N molecules at time 0, i.e. $R = N\delta(0, 0)$. Under such conditions, Eq.1 becomes:

$$\frac{\partial C}{\partial t} + \frac{\partial}{\partial x}(vC) = D\frac{\partial^2 C}{\partial x^2} + N\delta(0,0) \tag{2}$$

The solution to Eq.2 give us:

$$C(x,t) = \frac{N}{\sqrt{4\pi Dt}} \exp\left(-\frac{(x-vt)^2}{4Dt}\right) \tag{3}$$

which represents the channel impulse response (CIR).

Finally, assuming there is a passive receiver at position $\vec{x_r}$ with a molecular sensor volume V, the probability that the receiver detects the molecules as a function of time is:

$$p(t) = V \cdot C(x_r, t) \tag{4}$$

3 MC CHANNEL CHARACTERISTICS

In this section, we highlight key unique characteristics of the molecular communication channel that differ from traditional wireless and wired communication. We use the theoretical model of the channel presented in the previous section to explain these characteristics. Later in section 6, we empirically validate that this model is linear and fits the channel impulse response (CIR) we see in practice. We also validate all the characteristics presented here. Note however that our μ-Link decoder does not use the theoretical CIR equation for decoding. Instead, it directly estimates and updates the CIR without trying to do parameter fitting.

We introduce two new characteristics which have been overlooked by past work: *Non-causal ISI* and *Long delay spread vs. Coherence time*. We also highlight a third one, *signal dependant noise*. While it has been covered by past work [27, 31], it is an important to account for it in μ-Link.

3.1 Non-causal Inter-Symbol Interference

In communication systems, data bits are encoded into data symbols and transmitted over the channel. Inter-symbol interference (ISI) occurs when signals corresponding to different data symbols arrive at the same time at the receiver, which creates interference. In wireless RF communication, for example, ISI is mainly caused by multipath where signals from previously transmitted symbols travel along longer reflected paths and arrive late at the receiver interfering with later symbols. In such cases, ISI is *causal* i.e. only previous symbols can interfere with current and future symbols. Future symbols, on the other hand, cannot interfere with current or previous symbols since they cannot arrive earlier.

This, however, is not the case in molecular communication where due to the randomness of diffusion, molecules from future symbols can arrive earlier. As a result, the ISI is non-causal and both future and previous symbols can interfere with the current symbol. In particular, molecules of previous symbols can linger and arrive late creating interference with the current symbol, and molecules of future symbols can arrive earlier than molecules of the current symbol creating interference as well. Such non-causal ISI does not typically occur in other communication systems. To the best of our knowledge, it has never been addressed by past work in MC which limits the decoding performance.

To better understand this problem, consider the example in Fig. 2. Decoding achieves the highest confidence when the signal is sampled at its strongest, which is achieved around the peak of the channel impulse response. Let c_0 denote the peak of the unit pulse response as shown in Fig. 2a. Let $c_1, c_2, ..., c_M$ denote samples on the tail corresponding to molecules that arrive later and influence the following symbols which we call *forward-ISI*. Let $c_{-1}, c_{-2}, ..., c_{-F}$ denote samples on the head that arrive early and influence previous symbols which we call *backward-ISI*. Let b_k be the transmitted symbol, the sampled concentration r_k is:

$$r_k = \sum_{i=-\infty}^{\infty} c_i b_{k-i} \approx \sum_{i=-F}^{M} c_i b_{k-i} \tag{5}$$

Thus, to decode symbol b_k, we need to know the M previously transmitted symbols as well as the F future symbols.

[3] D is typically used as the notation of diffusion coefficient for molecular diffusion, while K is used for turbulent diffusion. For simplicity, we use D to represent both in this paper.

In RF communication, on the other hand, the following symbol can never arrive early before the current symbol as shown in Fig. 2b. Hence, to decode symbol b_k, we only need to know the previously transmitted symbols. This significantly simplifies the decoder since we can decode symbols sequentially which will give us the previously transmitted symbols. Furthermore, since wireless signals travel a the speed of light, ISI occurs only between consecutive symbols.

3.2 Long Delay Spread vs. Coherence Time

In communication systems, in order to correctly decode the bits, the channel impulse response (CIR) must be estimated and corrected for. The CIR has two key properties: delay spread and coherence time.

• **Delay Spread:** represents the length of the channel impulse response in time. In wireless communication, delay spread is mainly caused by multipath where the signal travels along different paths and arrives at different times at the receiver. In this case, the delay spread represents the time between the arrival of the first copy of the signal along the shortest path and the arrival of the last copy of the signal that is above the noise floor. However, since wireless signals travel at the speed of light, the difference in arrival time is typically of the order of nano to micro seconds. The delay spread also decreases as the distance between the transmitter and receiver increases since signals that travel along reflected paths start to arrive below the noise floor.

In contrast, delay spread in molecular communication is mainly caused by diffusion of molecules where different molecules arrive at different times at the receiver. Since diffusion is slow, legacy molecules tend to remain in the channel creating a very long tail. As a result, the delay spread can easily extend to multiple seconds. Fig. 3 shows an example of channel impulse response when the transmitter and receiver are 0.5, 1 and 2 meters apart. As can be seen, the delay spread can be as large as 2.5 seconds and expands as the distance increases, making the channel even harder to estimate.

• **Coherence Time:** corresponds to the time for which the channel impulse response can be considered fixed. In wireless communication, this is of the order of tens to hundreds of milliseconds which is orders of magnitude larger than the delay spread of the channel. Hence, it is possible to send a few training symbols at the beginning of a packet to estimate the CIR which can then be used to decode the bits throughout the packet. In molecular communication, however, the delay spread is of the same order as the channel coherence time. As a result, the channel changes as fast as the time it takes to estimate it. It is not possible to simply estimate the channel and use it to decode bits throughout the packet. Continuously estimating the channel, on the other hand, would result in a huge overhead that significantly reduces the data rate.

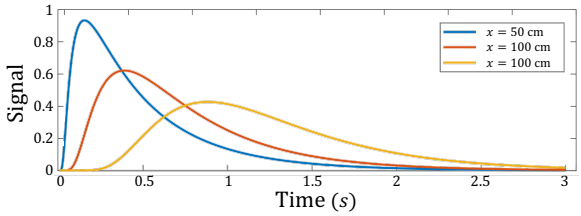

Figure 3: The molecular channel impulse response when the receiver is 50, 100, and 200 centimeters away from the transmitter.

3.3 Signal-Dependent Noise

The randomness of diffusion creates signal-dependent noise. In particular, the receiver will sample the concentration of molecules. Let r_k be the sampled concentration at the receiver, then $E[r_k] = \mu_k = C(x_R, k\Delta t)$ where x_R is the location of the receiver. In case of multiple symbols, μ_k is given by Eq. 5. Let N_k be the number of molecules at the receiver, then $N_k = V\mu_k$ where V is the detection volume of the receiver. The arrival of particles at the receiver follows a Poisson distribution with the same mean and variance. For tractability, the distribution can be approximated as Gaussian, i.e. $N_k \sim \mathcal{N}(V\mu_k, V\mu_k)$ [31]. Hence, the distribution of the sampled concentration r_k is:

$$r_k \sim \mathcal{N}\left(\mu_k, \frac{\mu_k}{V}\right) \tag{6}$$

The variance of the above distribution is proportional to the concentration. As a result, the noise in the signal is dependent on the signal itself and releasing more molecules to increase the signal strength increases the noise as well.

Compare this to wireless or wired communication where the noise is independent of the transmitted signal. There, the expectation of the distribution represents the signal whereas the variance represents the noise. The independence of noise has two important consequences. First, increasing the signal strength significantly increases the Signal-to-Noise Ratio (SNR). Second, maximum-likelihood decoders can be mapped into simple decision rules for demodulation (e.g. in BPSK, it is sufficient to check whether the real part of the symbol is positive or negative to decode "1" or "0" bit.) . However, such decoders designed for Additive White Gaussian Noise (AWGN) channel do not work well over the MC channel [31].

4 μ-LINK

This section describes the μ-Link communication protocol and decoder. μ-Link starts by sending a short preamble of known bits which are used for packet detection, channel estimation, and synchronization. The preamble is followed by data bits which are decoded using Hidden Markov Models and a Viterbi decoder customized to account for the specific characteristics of MC channels. μ-Link uses On-Off Keying and encodes a "1" bit by releasing molecules into the flow and a "0" by releasing nothing. Alg. 1 provides a high-level

pseudo-code for μ-Link's overall protocol and decoder. In the rest of this section, we describe μ-Link in detail.

4.1 Channel Estimation & Synchronization

Every μ-Link packet starts with a "1" bit, i.e. a pulse of molecules released into the liquid. The receiver constantly monitors the concentration of molecules and when it detects an increase in the signal strength i.e. concentration level, it triggers packet detection. However, due to the molecular channel, a transmitted pulse will result in a slow rise in concentration of molecules at the receiver followed by a slow drop with a very long tail as we have shown in Fig. 3. Hence, packet detection is likely to be triggered ahead of the peak signal strength of the transmitted symbol. It is important, however, to synchronize our decoder to the peak of the signal in order to maximize the SINR of each symbol.

Consider the example of the received signal, shown in blue, in Fig. 4. The channel impulse response (CIR) is shown in red which spans multiple symbols due to its long delay spread. If we synchronize our symbols to the first rise in signal strength, then the signal value will not properly represent the bit transmitted in each symbol. However, if we synchronize our symbols to the peak of the channel impulse response, then the signal value will be aligned with the bit transmitted in each symbol. This allows the decoder to achieve the highest confidence in decoding each bit since the signal is sampled at its strongest value with the minimal ISI , i.e. maximum SINR, as can be seen from the dotted red lines in Fig. 4.

In order to synchronize the decoder, we must first estimate the channel impulse response (CIR) to detect the peak of the signal. A simple approach is to start the preamble by transmitting a "1" bit followed by a lot of "0" bits. In principle, this would allow us to detect the peak. However, sending a single "1" bit results in a weak signal that is very susceptible to noise which compromises the accuracy of our channel estimation. Transmitting additional "1" bits in the preamble would increase the concentration of molecules making channel estimation more robust to noise which is needed for decoding data bits. Hence, μ-Link's preamble is formed of a "1" bit followed by a pseudo-random sequence of bits similar to the one shown in Fig. 4. The pseudo-random sequence improves the accuracy of channel estimation.

While μ-Link's design is driven by the theoretical channel model introduced in Eq. 3, μ-Link's channel estimation does not try to fit the estimated CIR to that model as it might not capture all practical constraints of the environment. Instead, μ-Link explicitly estimates the CIR using a Least Squares (LS) method. Specifically, the received signal can be written as $r(t) = c(t) * b(t)$ where $c(t)$ is the channel impulse response shown in Fig 3 and $b(t)$ is the sequence transmitted bits. For the preamble, we can rewrite the received samples in vector format as: $\mathbf{r} = \mathbf{Bc}$ where $\mathbf{B}$ is the Toeplitz matrix of the preamble bits and each column of $\mathbf{B}$ is a zero-padded version of the preamble bits. Thus, the LS estimator of $\mathbf{c}$ is:

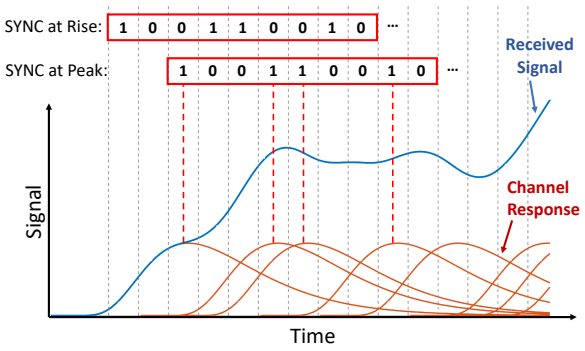

Figure 4: Blue curve depicts received signal without noise, while orange curve separates contribution of each bit. Synchronizing at the CIR peak will give higher SINR than the CIR start.

$$\tilde{\mathbf{c}} = (\mathbf{B}^T\mathbf{B})^{-1}\mathbf{B}^T\mathbf{r} \tag{7}$$

where $(\mathbf{B}^T\mathbf{B})^{-1}\mathbf{B}^T$ is the pseudo-inverse of $\mathbf{B}$.

After we estimate the channel $\mathbf{c}$, we can find the peak value of the CIR and align our decoder to the peak sample in $\mathbf{c}$. It is worth noting that the receiver can oversample $r(t)$ to improve decoding performance. In this case, $\mathbf{B}$ and $\mathbf{c}$ will represent oversampled versions of the preamble and the CIR.

4.2 Decoder

Decoding in molecular communication tends to be more complex than traditional wireless and wired systems. In particular, due to the long delay spread and non-causal ISI, each sampled value is a combination of many consecutive symbols including previous as well as future symbols which must all be jointly decoded. Moreover, widely adopted decoders for white Gaussian noise channels are non-optimal in molecular channels due to signal dependent noise. As a result, μ-Link adopts a Hidden Markov Model (HMM) to describe the molecular communication process and decodes using a sliding window block Viterbi algorithm.

4.2.1 Hidden Markov Model: Recall that in HMMs, a hidden Markov chain consists of an unknown sequence of states each of which probabilistically generates (emits) an observation. The observations are then used to infer the hidden states based on known transition and emission probabilities. In the context of μ-Link, the hidden states represent transmitted bits and the observations represent received signals.

μ-Link defines an HMM state s_k as a sequence of transmitted bits that contribute to the observation of the received signal r_k as shown in Fig. 5. As described in section 3.1, r_k is a combination the current bit, the M previous bits, and the F

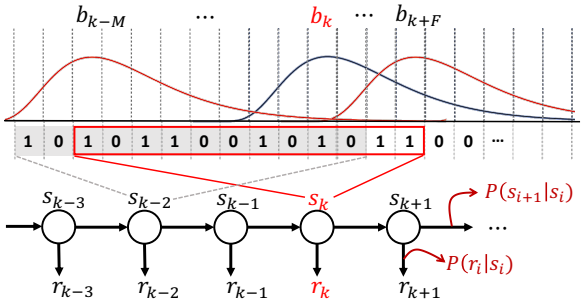

Figure 5: μ-Link's HMM where states represent a sliding window of bits accounting for both causal and non-causal ISI.

future bits weighted by the channel impulse response. Thus,

$$s_k = \{b_{k-M}, b_{k-M+1}, \cdots, b_k, \cdots b_{k+F}\}, \tag{8}$$

i.e., the HMM states represent a sliding window of $W = M + F + 1$ bits that account for both causal and non-causal ISI where W is the delay spread. M and F are computed based on the estimated channel impulse response. For example, the channel shown in Fig. 5 has $M = 8$ and $F = 3$.

The transition probability between states depends on the modulation and coding scheme being used. In case of On-OFF keying, each Markov state has only two valid transitions depending on whether the next bit to be added to the sliding window is a "0" or a "1". Thus, give an arbitrary state $s_i = \{s_i[1], \cdots, s_i[W]\}$, the state transition probability is:

$$P(s_{i+1}|s_i) = \begin{cases} \frac{1}{2} & s_{i+1} = \{s_i[2], \cdots, s_i[W], 0\} \\ \frac{1}{2} & s_{i+1} = \{s_i[2], \cdots, s_i[W], 1\} \\ 0 & otherwise \end{cases} \tag{9}$$

Moreover, given a channel impulse response $\mathbf{c}$ and an arbitrary state $s_i = \{s_i[1], \cdots, s_i[W]\}$, the emission or observation probability is defined as:

$$P(r_i|s_i) = \mathcal{N}\left(\mu_i, \frac{\mu_i}{V}\right) \tag{10}$$

which follows from Eq. 6 for signal dependent noise in MC channels. $\mathcal{N}$ is the normal (Gaussian) distribution, μ_i is the expected value of r_i given s_i and $\mathbf{c}$, and V is the detection volume at the receiver. μ_i can be written as:

$$\mu_i = \sum_{j=-F}^{M} c_j s_i[M + 1 - j] \tag{11}$$

4.2.2 Block Viterbi Algorithm: The above HMM is solved using a block Viterbi decoder which returns the maximum-a-posteriori (MAP) solution of the Markov state transition sequence, i.e. the solution that maximizes the joint probability $P(s_1, \cdots, s_L, r_1, \cdots, r_L)$ where L is the total number of bits being decoded. The Viterbi decoder uses the following

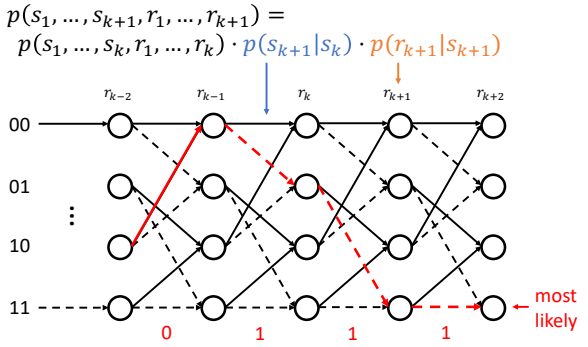

Figure 6: A simple example of a Viterbi decoding graph. Blue arrow points to transmission probability (hidden state), the orange points to emission probability (signal-dependent noise), and the red indicate the most likely path.

dynamic programming equation to solve the problem:

$$P(s_1, \cdots, s_{k+1}, r_1, \cdots, r_{k+1}) = \max\{P(s_1, \cdots, s_k, r_1, \cdots, r_k) P(s_{k+1}|s_k) P(r_{k+1}|s_{k+1})\}$$

Fig. 6 shows a simplified example of the Viterbi decoder for $W = 2$ where the most likely path is highlighted in red. However, for practical MC channels, W can easily exceed 10, similar to Fig. 5 where $W = 12$. The number of states in the Viterbi graph is 2^W. Thus, the Viterbi decoder requires $O(L2^W)$ memory and computation which for a 100 bit packet with $W = 12$ results in $> 400,000$ operations. To address this, we incrementally build the Viterbi decoding graph starting from the preamble and accounting only for valid transitions and the K highest probability states where K is a tunable parameter. Hence, only the top K states are considered at every stage of the Viterbi decoder which reduces the number of operations to $O(LK)$ resulting in a practical decoder complexity. For example, in our evaluation, when $W = 12$ and we have 4096 states, we set $K = 128$. Furthermore, due to the use of a sliding window, the decoder does not need to memorize all the columns in the Viterbi graph shown in Fig. 6. Instead, it is sufficient to store the F previous columns which reduces the memory requirement to $O(FK)$. This allows μ-Link to efficiently adapt to longer packet lengths (i.e. larger L) and MC channels with longer delay spread (i.e. larger W).

4.2.3 Channel Tracking. The above μ-Link decoder accounts for non-causal ISI, long delay spread, and signal dependent noise. However, it assumes that the channel impulse response is known and fixed. This is not true in MC channels where the channel coherence time is of the same order as the delay spread. Thus, the time it takes to estimate the channel is only slightly longer than the time it takes for the channel to change. Re-estimating the channel, by sending more preamble or pilot bits, would result in a huge overhead since the CIR is very long and we can only send a few data bits before we need to estimate the channel again.

Algorithm 1 μ-Link Protocol & Decoder Pseudo-code

1: $\mathbf{r} \leftarrow$ sampled signal at receiver.
2: $\mathbf{b_p} \leftarrow$ known preamble bits.
3: $t_{start} \leftarrow$ PacketDetection($\mathbf{r}$)
4: $\mathbf{c} \leftarrow$ ChannelEstimate($\mathbf{r}, \mathbf{b_p}, \mathbf{t_{start}}$)
5: $M, F \leftarrow$ GetISI($\mathbf{c}$)
6: $W \leftarrow M + F + 1$
7: **HMM** $\leftarrow$ Viterbi.init($M, F, \mathbf{r}, \mathbf{b}_p, K$)
8: $t_{sync} \leftarrow$ Sync($\mathbf{r}, \mathbf{c}, \mathbf{t_{start}}$)
9: $i \leftarrow t_{sync} + length(\mathbf{b}_p)$
10: **while** $i < L$ **do**
11: // Viterbi Forward Pass
12: **HMM** $\leftarrow$ Viterbi.updateProb(**HMM**, $\mathbf{r}[i], \mathbf{c}, K$)
13: // Viterbi Backward Pass
14: $\tilde{\mathbf{b}}[i-F] \leftarrow$ Viterbi.decode(**HMM**)
15: **if** $i \mod T = 0$ **then**
16: $\mathbf{c} \leftarrow$ Viterbi.channelTrack($\mathbf{c}, \tilde{\mathbf{b}}, \mathbf{r}$)
17: $i \leftarrow i + 1$

μ-Link tracks the CIR throughout the packet without sending any additional preamble or pilot bits. To do so, μ-Link outputs the decoding results of the Viterbi dynamic programming algorithm without waiting till the end of the sequence as shown in line 14 of Alg. 1. After every T iterations of the Viterbi algorithm, μ-Link uses the decoded bits as a ground truth to re-estimate the channel impulse response. In order to minimize errors, μ-Link adopts the following:

(1) It leverages the soft values (probabilities) of the window blocks of decoded bits as a decoding confidence metric to decide which bits should be used for re-estimation.
(2) It avoids the last F bits for which the decoded values can not yet be trusted due to non-causal ISI from the current and futures bits that have not been decoded.
(3) It rejects new CIR estimates that vary significantly from the most recent CIR estimate. In particular, if wrongly decoded bits are used, the CIR will exhibit huge changes that do not match the diffusion model of MC.

The above criteria ensures that μ-Link generates reliable estimates of the channel throughout the packet.

5 TESTBED

In order to evaluate μ-Link and our insights into the MC channel, we build an MC experimental platform shown in Fig. 1 and Fig. 7. The testbed follows a similar approach to past experimental testbeds on validating the molecular communication channel [19, 60]. The testbed is built up with common and non-harmful materials, and can be divided into three parts: channel, transmitter and receiver.

• **Channel**: The channel is mainly formed of a network of tubes with flowing water. A background pump continuously delivers water into the tubes to maintain a stable flow from the transmitter to the receiver and propel the propagation of molecules. The path between TX and RX is not limited to the single tube shown in Fig. 7, but can be a combination of tubes/paths as shown in Fig. 1.

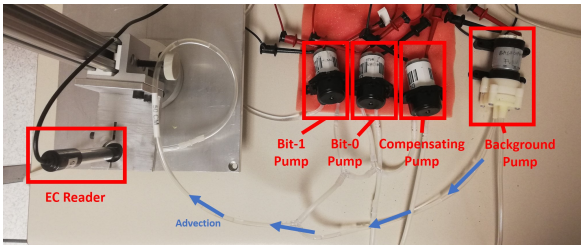

Figure 7: A Molecular Communication Testbed with a single path.

• **Transmitter**: The transmitter is composed of three peristaltic pumps: two data pumps and one compensation pump. The data pumps either inject saline solution to encode a "1" bit or pure water to encode a "0" bit. During a symbol interval, the data pumps only inject liquid for 50 ms. The compensation pump will inject water for the remaining time in the symbol interval in order to compensate for flow variation.

• **Receiver**: The receiver uses an EC (electrical conductivity) reader, controlled by an Arduino board. The value output by the ADC is linearly related to the EC value which is in turn linearly related to the concentration of salt.

6 EVALUATION

In this section, we start by validating the characteristics of the molecular communication channel presented in this paper. We then evaluate the performance of μ-Link and compare it tp past work. Finally, we provide some micro-benchmarks that give insights into μ-Link's performance.

6.1 Channel Validation

We start by providing results and illustrative examples that validate the diffusion channel model presented in Eq. 3, the linearity of the channel, the signal dependent noise, the delay spread and the non-causal ISI.[4]

6.1.1 Diffusion Channel Model. Fig.8 provides a model fitting of the channel model in Eq. 3 to a channel impulse response measured on our testbed in which the receiver is at a distance $x = 0.25m$ from the transmitter. We fit the CIR parameters as $v = 0.33m/s$ and $D = 0.025m^2/s$. The figure shows that the testbed provides a good platform for molecular communication that incorporates the advection-diffusion properties and closely matches the theoretical model. However, the equation cannot fully capture

[4]The channel coherence time property will be evaluated in section 6.3 by showing that if we do not track the changing channel frequently enough, our decoding performance will suffer.

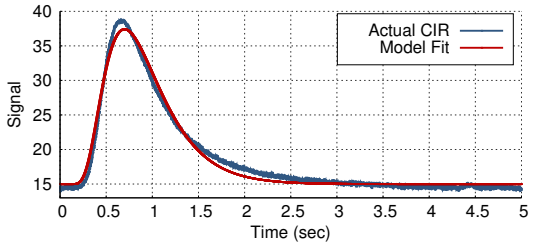

Figure 8: Curve fitting for single-tube MC channels to Eq. 3.

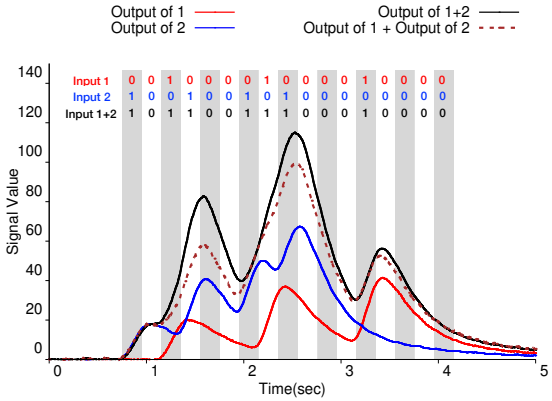

Figure 9: Channel linearity validation experiment. The sum of signals by two complementary sequences roughly match the signal by the sum of these two sequences.

some of the hard to model properties in practical testbeds, such as, the non-uniformity of diffusion and turbulence throughout the testbed.

6.1.2 Linearity. Our design as well as Eq. 5 assume that the receiver is linear, i.e. the measured concentration is a sum of the concentrations resulting from individually transmitted bits. To verify this assumption, we transmit 3 sequences of bits: S_1, S_2, and S_3 and measure the received signals R_1, R_2, and R_3 respectively. S_1 and S_2 are two random sequences with non-overlapping "1"s shown in red and blue in Fig. 9. $S_3 = S_1 + S_2$ and is shown in black. If the model is linear, then we should get $R_3 = R_1 + R_2$. Fig. 9 plots R_1, R_2, R_3, and $R_1 + R_2$ after averaging them over multiple runs to eliminate noise. The figure shows that R_3 closely matches $R_1 + R_2$. While the curves do not perfectly match, the approximation is sufficient to yield good performance in practice.

6.1.3 Signal-Dependent Noise. To measure the noise in the channel, we send a pulse followed by a long sequence of zeros to directly compute the channel shown on the top of Fig. 10. We repeat the measurement many times and compute the variance at each point of the channel across the measurements which we denote as the noise. Fig. 10 plots the noise power as a function of the signal power. While we cannot separate thermal Gaussian noise from signal-dependent noise, the graph clearly shows that higher signal power leads

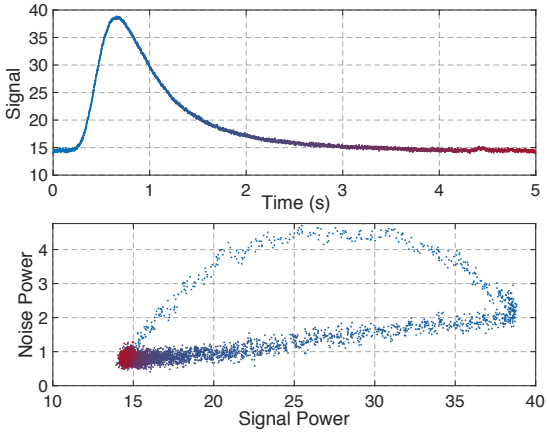

Figure 10: SDN validation experiment. CIR is computed from data between manually synchronized transmitter and receiver. Noise of each CIR sample is plotted in the same color of the sample.

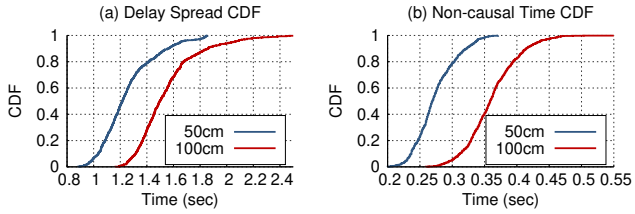

Figure 11: Delay spread and non-causality statistics. For 100 cm molecular channel, information particles takes longer time to propagate from transmitter to receiver, so diffusion takes more proportion in CIR and makes more ISI than 50 cm channel.

to a higher noise variance indicating that the noise is dependent on the signal. Note that the signal dependent noise is higher in the samples corresponding to the rising head of the CIR likely due to imperfections in the transmitter pumps.

6.1.4 Long Delay Spread and Non-causality ISI. Fig.11 empirically validates the long delay spread and non-causality properties of the molecular channel. After estimating each channel with the preamble, the delay spread is computed as the period from when the CIR first reaches 10% of the peak value until it drops below 10%. Similarly, the non-causal ISI duration is computed as the period from when CIR first reaches 10% of the peak value until it achieves the maximum peak. Fig.11 plots the CDF of the delay spread and the non-causal ISI duration for when the receiver is 50 cm and 100 cm away from the transmitter. The median delay spread is 1.2s at 50 cm and increases to 1.5s at 100 cm which spans 12 and 15 symbols at a bit rate of 10 bps. The maximum, however, can reach 2.4s which would create ISI for 24 symbols at 10 bps. The median non-causal ISI duration is 0.27 sec and 0.36 sec for 50 cm and 100 cm respectively which affects 2 - 4 symbols at 10 bps. As we increase the bit rate, the influence of ISI extends to more symbols which presents a major obstacle for improving the data rate in MC.

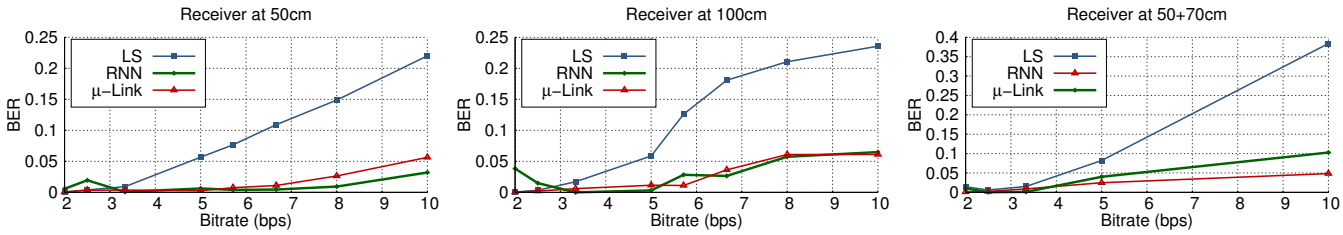

Figure 12: μ-Link LS and RNN performance on single-path channel of 50 cm (left) and 100 cm (middle), and on two-path channel of 50 cm and 70 cm (right). μ-Link and RNN achieves comparable performance, and show great advantage over LS decoder.

6.2 μ-Link's Performance

In this section, we evaluate the performance of μ-Link.

6.2.1 Baselines. We compare μ-Link to two state-of-the-art decoding techniques:

- **Least Square (LS) Decoder:** The LS decoder is very similar to the LS channel estimation introduced in Sec. 4. The main difference is that now we know the CIR and wish to estimate the bits. Hence, we write the CIR into Toeplitz matrix $\mathbf{C}$ and multiply its pseudo-inverse with the received samples to get the LS solution $\tilde{\mathbf{b}} = (\mathbf{C}^T\mathbf{C})^{-1}\mathbf{C}^T r$.
- **RNN decoder:** Recent work in [18] leveraged Recurrent Neural Networks (RNN) to decode MC. Specifically, [18] uses Long Short-Term Memory (LSTM) which is especially good at processing time sequences. The LSTM uses a sliding window for decoding and has a bi-directional structure, i.e. the sequence is analyzed in both forward and backward directions. We implement and train the bi-directional LSTM using the same neural network architecture and parameters described in [18].

6.2.2 Dataset. We collect a large dataset of molecular signals. Our dataset includes sequences with varying symbol interval (i.e. bit rate) and distance between transmitter and receiver. The dataset is divided into two parts. The first is for single-path channel shown in Fig. 7. We test for distances of 25, 50 and 100 cm. The second part of the dataset is for a two-path channel shown in Fig. 1. The paths have distances of 50 and 70 cm. In both parts, we vary the symbol interval between 100 and 500 ms which translates to bit rates ranging from 2 to 10 bps. For each experiment, we transmit 100 different sequences, each containing 100 bits. For the RNN decoder, 70% of the dataset is used for training.

6.2.3 Results. Fig. 12 summarizes the average BER performance as a function of bit rate for all three decoders: μ-Link, LS, and RNN. As expected, the BER degrades as the bit rate increases, i.e. the symbol length decreases. However, the LS decoder shows a major increase in BER with increasing bit rate where at 10 bps the BER is above 20% for the single path channels and 37% for the two path channel. The BER degradation in case of μ-Link and the RNN is significantly less. For the single path channels at 10 bps, μ-Link and the RNN achieve a BER of around 5%. However, for the two path channel at 10 bps, μ-Linkachieves a BER of 5% whereas the RNN achievers a BER of 10%. Compared with single-path, a two-path channel incurs longer delay spread and more ISI. This is because the same amount of flow splits into two tubes, decreasing the flow velocity and increasing propagation time. In such a case, μ-Link's explicit CIR estimation outperforms the RNN's ability to implicitly account for the channel.

The advantage of μ-Link over the RNN is further emphasized once we consider the RNN's need for offline training on a large dataset specific to the channel. Training for one kind of channel is unlikely to generalize to other and possibly more complicated channels. To verify this, we run an experiment where we train the RNN for specific channels and test it on different channels in the dataset. Specifically, we omit data for certain distances or bit rates from the training set. Fig. 13 shows the performance of the RNN using different training sets but the same testing set on single-path channel. For the training set:

- "all dist" refers to distances of 25, 50, and 100 cm.
- "all rate" refers to bit rates: 2, 2.5, 3.3, 5, 5.7, 6.7, 8 & 10 bps.
- "some dist" refers to 25 and 50 cm only.
- "some rate" refers to bit rates: 2, 2.5, 3.3, 5, & 10 bps.

Fig. 13 shows that the performance of the RNN is good only if the training set contains "all dist + all rate" which covers all possible channels in the data set. However, as soon as, "some dist" or "some rate" are not in the training set, the RNN performance is extremely poor. For example, in the case "some dist + all rate", the RNN constantly performs worse with BER larger than 15% at bit rates above 5 bps. In the case of "all dist + some rate", the figure shows that the RNN performs well for rates that are included in the training set such as 3.3, 5, and 10 bps and performs very poorly for rates that are not in the training set such as 5.7, 6.7, and 8 bps where the BER is larger than 20%. Thus, while RNNs can be useful for decoding MC, they require training for all possible channels and bit rates which is not practical.

Finally, μ-Link is able to significantly improve the BER and the achievable bit rates compared to LS decoding. It is able to achieve comparable performance to the RNN when

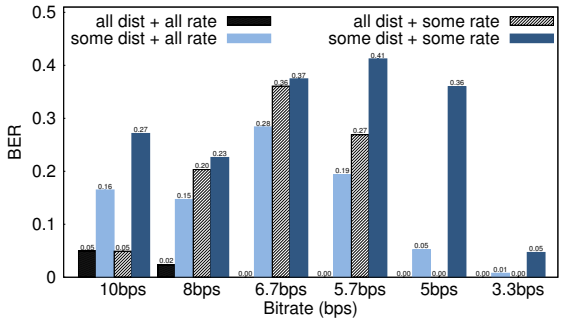

Figure 13: RNN overfitting issue. Four RNN model with partially (or no) missing dataset are tested on the same sequences.

the RNN's training set contains all channels and bit rates. However, significantly outperforms the RNN if the RNN is not trained for the specific channel and bit rate. Specifically, μ-Link can improve the data rate and reduce the bit errors to achieve 5 - 10 bps with 0.2% - 5% BER. Compared to the state-of-the-art experimental results reported in the RNN paper [18], μ-Link achieves 2.5× higher bit rate for the same BER or 20× lower BER for the same bit rate without the need to train and use deep neural networks.

6.3 Microbenchmarks

In this section, we present two microbenchmarks that give us insight into the importance of addressing the two new characteristics of MC channels presented in this paper. Figure 14 shows the performance of μ-Link with and without its design components for addressing non-causal ISI and channel coherence time. The figure shows three curves: μ-Link μ-Link without CU (Channel Update), μ-Link without NC (Non-causal ISI) and CU. The figure shows the average BER versus the bit rate at 50 cm distance between the transmitter and receiver. At a bit rate of 10 bps, μ-Link achieves a BER of 5%. However, this BER degrades to 22% if we do not track and update the channel and further to 29% if we do not account for non-causal ISI. This shows why past work that does not incorporate such insights remains limited in achievable bit rate to less than 4 bps.

Fig.15 shows the performance of μ-Link as function of the frequency of tracking and updating the channel, i.e. parameter T in Alg. 1. The figure shows that the more frequently we update the channel (smaller update interval T), the lower the BER. This is particularly important for higher bit rates where the symbol interval is smaller. There, the contribution of ISI to many symbols becomes more prominent and having good estimates of the channel impulse response is necessary to ensure reliable decoding. For example, at 10 bps, where the delay spread (ISI) spans 12 symbols, updating the channel every 10 bits yields a BER of 5% which increases to 18.6% if we update it every 50 bits. Hence, channel coherence time is of the same order as the delay spread which presents a

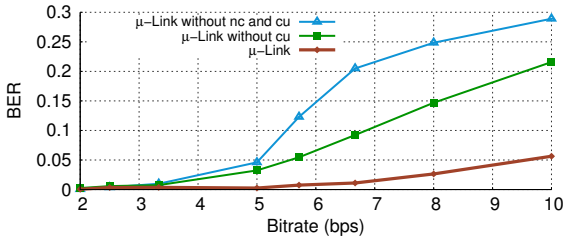

Figure 14: Importance of accounting for non-causal ISI (nc) and tracking the channel (cu) in μ-Link.

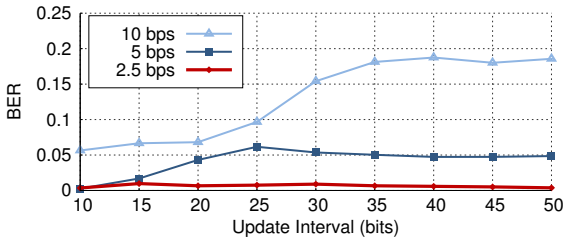

Figure 15: Importance of quickly tracking the channel in μ-Link.

bottleneck for improving the bit rate in MC channels. By tracking the channel, μ-Link is able to significantly improve the BER for higher bit rates.

7 RELATED WORK

In this section, we present further background and related work on molecular communication. As mentioned before, for a thorough literature review, we refer the reader to the following surveys [4, 20, 34].

A. MC Channel Modeling and Estimation: There has been a significant amount of work on modeling the MC channel taking into account different factors such as propagation environment, dimensions (1D, 2D, 3D), external influences like turbulence and advection, mobility, and type of receiver (destructive vs non-destructive) [15, 16, 47, 59, 65, 68]. Time varying channel due to mobility is also modeled in [11, 62]. However, the models do not account for other time varying factors such as unstable advection that can be caused by pumping. A number of papers also focus on estimating the channel parameters such as distance, diffusion coefficient and fitting them to to a known model or closed-form expression [27, 46, 58]. Unfortunately, all these works are based on simulations and none of them are validated in practice. While modeling provides valuable insights, it cannot account for all factors and parameters that can influence the channel in practice as shown in [60]. In this paper, we use theoretical models and empirical experimentation to guide our understanding of the channel and introduce new characteristics. However, for decoding, we do not attempt to parameter fit our estimate to a closed form model but rather directly estimate the channel impulse response.

B. MC Channel Capacity: There has been theoretical work on studying the capacity of molecular communication [6, 7, 36, 37, 49]. However, to derive the capacity of the channel, these works must make simplifying assumptions that do not hold in practice. [36, 37] derive the MC channel with mobile transmitter or receiver but completely ignore ISI. [6, 7] consider signal dependent noise but assume a static channel. [49] considers signal dependent noise and ISI but assumes propagation through diffusion only. None account for non-causal ISI. Deriving the capacity is, indeed, valuable for understanding the data rate limits of MC. However, the channels tend to be significantly more complex in practice.

C. MC Decoders (Simulations): Several MC decoders have been introduced and tested using simulations. Some exploit specific features of the MC channel response like monotonicity and local convexity [35, 67] but assume minimal ISI. Others introduce optimal decoders [31, 42, 45] but assume the channel impulse response is perfectly known a priori. [29] introduced a non-coherent decoder using blind channel estimation but it treats ISI as noise. These decoder are tested only in simulations and underestimated the severity of ISI in practice especially as we go to shorter symbols (higher data rates). Furthermore, they do not address non-causal ISI and the long delay spread vs. coherence time.

Some theoretical work tries to address the severity of forward-ISI in MC channel using mechanisms to reduce the tail of the channel impulse response. Some propose using enzymes or photolysis reactions to remove interfering molecules retained in the channel [13, 44] while others propose using magnetic molecules and adding an external magnetic field [63, 64]. These methods, however, have not been tested in practice and can only reduce forward-ISI but not eliminate it. μ-Link, on the other hand, aims to decode in the presence of both forward and backward ISI.

D. MC Experimental Work: Unlike theoretical and simulation based past work, there are very few experimental MC testbeds especially in liquids. Most MC testbeds are for airborne molecular communication where the molecules are released in air [25, 32, 33, 39, 48, 50]. The dynamics of molecular propagation in such gaseous mediums tend to be significantly different than liquids. The applications of airborne MC also tend to be limited since wireless RF works really well in air. In this paper, we focus on liquid-based molecular communication for which very few testbeds exist [19, 24, 60]. All testbeds use water as the liquid. For molecules, they use magnetic particles [60], RNA [24] and acid/base [19]. [24, 60] focus on channel modeling and fitting and do provide an evaluation of data rate or BER. [60] uses a symbol interval 4s corresponding to 0.25 bps data rate whereas [24] does not report symbol interval or data rate.

The closest to our work is [19] which uses deep neural network techniques including LSTM RNN to decode without explicitly modeling or estimating the channel. While it achieves good performance, it relies heavily on tedious training for every distance, channel, and bit rate. Hence, it suffers from overfitting as we have show in section 6 and cannot deal with new channels and new bit rates that it has not seen before. μ-Link, on the other hand, is able to achieve better performance by properly modeling the characteristics of the MC channel without relying on neural networks.

8 LIMITATIONS & FUTURE WORK

This paper only takes the first steps towards better understanding of the molecular communication channel. We believe the paper provides valuable insights that are driven by theoretical models, simulations, and experimentation. However, the empirical validation of these insights is limited to our testbed. Further experimental research is required which will enable more accurate channel models and new insights. In this section, we outline some of the limitations of the current system and future directions for this project.

- **In-Vitro Testbed:** The current testbed is limited. In particular, a more elaborate network of tubes, connections, and pumps that better resemble the circulatory system should be adopted. Moreover, testing on different types of molecules, receivers, and fluids, other than water, with different diffusion coefficients should be conducted.
- **Linearity:** While both theoretical and empirical results show that the MC channel is linear, the linearity of the sampled MC signal itself largely depends on the choice of receiver. In our testbed, we make sure that all our received signals fall in the linear range of the EC meter. However, this linearity might not be guaranteed for all types of molecules and corresponding receivers.
- **Modulation & Coding:** In this paper, we only consider OOK modulation without any coding since our main goal is to understand the MC channel. Further research is needed to explore different modulation and coding schemes that could enhance the performance of MC.
- **In-Vivo Experiments:** A future goal of this work is to validate the channel model in-vivo thought animal testing for micro-implants and micro-fluids in wet-labs. Such experiments might reveal new and different challenges in MC that would require further research.
- **Mobility:** The insights and system developed in this paper only applies to static transceivers. However, in some applications like targeted drug delivery, the device might move through the bloodstream resulting in abrupt or hard to track channel variations. Such changes are not captured by our system and are left for future work.

REFERENCES

[1] [n.d.]. Mass Transport Processes. https://pages.mtu.edu/~reh/courses/ce251/251_notes_dir/node4.html. (Accessed on 03/24/2020).

[2] Nastaran Abadi, Amin Aminzadeh Gohari, Mahtab Mirmohseni, and Masoumeh Nasiri-Kenari. 2018. Zero-error codes for multi-type molecular communication in random delay channel. In *IWCIT 2018 - Iran Workshop on Communication and Information Theory*. IEEE, 1–6. https://doi.org/10.1109/IWCIT.2018.8405050

[3] Arman Ahmadzadeh, Vahid Jamali, and Robert Schober. 2018. Stochastic channel modeling for diffusive mobile molecular communication systems. *IEEE Transactions on Communications* 66, 12 (2018), 6205–6220.

[4] Ozgur B. Akan, Hamideh Ramezani, Tooba Khan, Naveed A. Abbasi, and Murat Kuscu. 2017. Fundamentals of molecular information and communication science. *Proc. IEEE* 105, 2 (feb 2017), 306–318. https://doi.org/10.1109/JPROC.2016.2537306

[5] Ian F. I.F. Akyildiz, Youssef Chahibi, Massimiliano Pierobon, Sang Ok Song, and Ian F. I.F. Akyildiz. 2013. A molecular communication system model for particulate drug delivery systems. *IEEE Transactions on Biomedical Engineering* 60, 12 (dec 2013), 3468–3483. https://doi.org/10.1109/TBME.2013.2271503

[6] Gholamali Aminian, Hamidreza Arjmandi, Amin Gohari, Masoumeh Nasiri Kenari, and Urbashi Mitra. 2015. Capacity of LTI-poisson channel for diffusion based molecular communication. In *2015 IEEE International Conference on Communications (ICC)*. IEEE, 1060–1065.

[7] Gholamali Aminian, Hamid Ghourchian, Amin Gohari, Mahtab Mirmohseni, and Masoumeh Nasiri-Kenari. 2017. On the capacity of signal dependent noise channels. In *2017 Iran Workshop on Communication and Information Theory (IWCIT)*. IEEE, 1–6.

[8] Hamidreza Arjmandi, Amin Gohari, Masoumeh Nasiri Kenari, and Farshid Bateni. 2013. Diffusion-based nanonetworking: A new modulation technique and performance analysis. *IEEE Communications Letters* 17, 4 (apr 2013), 645–648. https://doi.org/10.1109/LCOMM.2013.021913.122402 arXiv:arXiv:1209.5511v1

[9] Youssef Chahibi, Ian F. Akyildiz, Sasitharan Balasubramaniam, and Yevgeni Koucheryavy. 2015. Molecular Communication Modeling of Antibody-Mediated Drug Delivery Systems. *IEEE Transactions on Biomedical Engineering* 62, 7 (2015), 1683–1695. https://doi.org/10.1109/TBME.2015.2400631

[10] Youssef Chahibi, Massimiliano Pierobon, and Ian F. Akyildiz. 2015. Pharmacokinetic modeling and biodistribution estimation through the molecular communication paradigm. *IEEE Transactions on Biomedical Engineering* 62, 10 (oct 2015), 2410–2420. https://doi.org/10.1109/TBME.2015.2430011

[11] Ge Chang, Lin Lin, and Hao Yan. 2017. Adaptive detection and ISI mitigation for mobile molecular communication. *IEEE Transactions on nanobioscience* 17, 1 (2017), 21–35.

[12] James E Dahlman, Kevin J Kauffman, Yiping Xing, Taylor E Shaw, Faryal F Mir, Chloe C Dlott, Robert Langer, Daniel G Anderson, and Eric T Wang. 2017. Barcoded nanoparticles for high throughput in vivo discovery of targeted therapeutics. *Proceedings of the National Academy of Sciences* (2017), 201620874.

[13] Oussama Abderrahmane Dambri and Soumaya Cherkaoui. 2018. Enhancing Signal Strength and ISI-Avoidance of Diffusion-based Molecular Communication. In *2018 14th International Wireless Communications & Mobile Computing Conference (IWCMC)*. IEEE, 1–6.

[14] Yansha Deng, Adam Noel, Maged Elkashlan, Arumugam Nallanathan, and Karen C. Cheung. 2016. Modeling and Simulation of Molecular Communication Systems with a Reversible Adsorption Receiver. *IEEE Transactions on Molecular, Biological and Multi-Scale Communications* (2016), 1–1. https://doi.org/10.1109/TMBMC.2016.2589239 arXiv:1601.00681

[15] Fatih Dinc, Bayram Cevdet Akdeniz, Ecda Erol, Dilara Gokay, Ezgi Tekgul, Ali Emre Pusane, and Tuna Tugcu. 2018. Analytical Derivation of the Impulse Response for the Bounded 2-D Diffusion Channel. (sep 2018). arXiv:1809.08784 http://arxiv.org/abs/1809.08784

[16] Fatih Dinc, Bayram Cevdet Akdeniz, Ali Emre Pusane, and Tuna Tugcu. 2018. A General Analytical Solution to Impulse Response of 3-D Microfluidic Channels in Molecular Communication. *arXiv preprint arXiv:1804.10071* (2018).

[17] Md Fakruddin, Zakir Hossain, and Hafsa Afroz. 2012. Prospects and applications of nanobiotechnology: a medical perspective. *Journal of nanobiotechnology* 10, 1 (2012), 31.

[18] Nariman Farsad and Andrea Goldsmith. 2018. Neural Network Detection of Data Sequences in Communication Systems. (jan 2018). https://doi.org/10.1109/TSP.2018.2868322 arXiv:1802.02046

[19] Nariman Farsad, David Pan, and Andrea Goldsmith. 2018. A novel experimental platform for in-vessel multi-chemical molecular communications. In *2017 IEEE Global Communications Conference, GLOBECOM 2017 - Proceedings*, Vol. 2018-Janua. IEEE, 1–6. https://doi.org/10.1109/GLOCOM.2017.8255058 arXiv:1704.04810

[20] Nariman Farsad, H. Birkan Yilmaz, Andrew Eckford, Chan-Byoung Chae, and Weisi Guo. 2014. A Comprehensive Survey of Recent Advancements in Molecular Communication. *IEEE Communications Surveys & Tutorials* 18, 3 (2014), 1887–1919. https://doi.org/10.1109/COMST.2016.2527741 arXiv:1410.4258

[21] Luca Felicetti, Mauro Femminella, and Gianluca Reali. 2015. Smart Antennas for Diffusion-based Molecular Communications. *Proceedings of the Second Annual International Conference on Nanoscale Computing and Communication* September (2015), 27:1—-27:6. https://doi.org/10.1145/2800795.2800817

[22] Luca Felicetti, Mauro Femminella, and Gianluca Reali. 2017. Congestion Control in Molecular Cyber-Physical Systems. *IEEE Access* 5 (2017), 10000–10011. https://doi.org/10.1109/ACCESS.2017.2707597

[23] Luca Felicetti, Mauro Femminella, Gianluca Reali, Tadashi Nakano, and Athanasios V. Vasilakos. 2014. TCP-like molecular communications. *IEEE Journal on Selected Areas in Communications* 32, 12 (dec 2014), 2354–2367. https://doi.org/10.1109/JSAC.2014.2367653 arXiv:1406.4259

[24] Taro Furubayashi, Yoshihiro Sakatani, Tadashi Nakano, Andrew Eckford, and Norikazu Ichihashi. 2018. Design and wet-laboratory implementation of reliable end-to-end molecular communication. *Wireless Networks* 24, 5 (jul 2018), 1809–1819. https://doi.org/10.1007/s11276-016-1435-4

[25] Stamatios Giannoukos, Daniel Tunç McGuiness, Alan Marshall, Jeremy Smith, and Stephen Taylor. 2018. A Chemical Alphabet for Macromolecular Communications. *Analytical Chemistry* 90, 12 (jun 2018), 7739–7746. https://doi.org/10.1021/acs.analchem.8b01716

[26] Weisi Guo, Taufiq Asyhari, Nariman Farsad, H. Birkan Yilmaz, Bin Li, Andrew Eckford, and Chan Byoung Chae. 2016. Molecular communications: Channel model and physical layer techniques. *IEEE Wireless Communications* 23, 4 (aug 2016), 120–127. https://doi.org/10.1109/MWC.2016.7553035 arXiv:1507.07292

[27] Vahid Jamali, Arman Ahmadzadeh, Christophe Jardin, Heinrich Sticht, and Robert Schober. 2016. Channel Estimation for Diffusive Molecular Communications. In *IEEE Transactions on Communications*, Vol. 64. 4238–4252. https://doi.org/10.1109/TCOMM.2016.2601098 arXiv:1510.08612

[28] Vahid Jamali, Arman Ahmadzadeh, Wayan Wicke, Adam Noel, and Robert Schober. 2018. Channel Modeling for Diffusive Molecular Communication - A Tutorial Review. (dec 2018). arXiv:1812.05492

http://arxiv.org/abs/1812.05492

[29] Vahid Jamali, Nariman Farsad, Robert Schober, and Andrea Goldsmith. 2016. Non-Coherent Multiple-Symbol Detection for Diffusive Molecular Communications. *Proc. ACM NANOCOM* (2016), 1–7. https://doi.org/10.1145/2967446.2967466 arXiv:1707.08926

[30] Oliver Jonas, Heather M Landry, Jason E Fuller, John T Santini, Jose Baselga, Robert I Tepper, Michael J Cima, and Robert Langer. 2015. An implantable microdevice to perform high-throughput in vivo drug sensitivity testing in tumors. *Science translational medicine* 7, 284 (2015), 284ra57—-284ra57.

[31] Deniz Kilinc and Ozgur B. Akan. 2013. Receiver design for molecular communication. *IEEE Journal on Selected Areas in Communications* 31, 12 (2013), 705–714.

[32] Na-Rae Kim, Nariman Farsad, Changmin Lee, Andrew W. Eckford, and Chan-Byoung Chae. 2019. An Experimentally Validated Channel Model for Molecular Communication Systems. *IEEE Access* 7 (2019), 1–1. https://doi.org/10.1109/access.2018.2889683

[33] Bon Hong Koo, Changmin Lee, H. Birkan Yilmaz, Nariman Farsad, Andrew Eckford, and Chan Byoung Chae. 2016. Molecular MIMO: From Theory to Prototype. *IEEE Journal on Selected Areas in Communications* 34, 3 (mar 2016), 600–614. https://doi.org/10.1109/JSAC.2016.2525538 arXiv:1603.03921

[34] Murat Kuscu, Ergin Dinc, Bilgesu A. Bilgin, Hamideh Ramezani, and Ozgur B. Akan. 2019. Transmitter and Receiver Architectures for Molecular Communications: A Survey on Physical Design with Modulation, Coding and Detection Techniques. *Proc. IEEE* 107, 7 (jul 2019), 1302–1341.

[35] Bin Li, Mengwei Sun, Siyi Wang, Weisi Guo, and Chenglin Zhao. 2016. Local Convexity Inspired Low-Complexity Noncoherent Signal Detector for Nanoscale Molecular Communications. *IEEE Transactions on Communications* 64, 5 (may 2016), 2079–2091. https://doi.org/10.1109/TCOMM.2016.2543734 arXiv:1508.07075

[36] Lin Lin, Qian Wu, Fuqiang Liu, and Hao Yan. 2018. Mutual Information and Maximum Achievable Rate for Mobile Molecular Communication Systems. *IEEE Transactions on Nanobioscience* 17, 4 (2018), 507–517. https://doi.org/10.1109/TNB.2018.2870709

[37] Zhan Luo, Lin Lin, Qi Fu, and Hao Yan. 2018. An Effective Distance Measurement Method for Molecular Communication Systems. In *2018 IEEE International Conference on Sensing, Communication and Networking (SECON Workshops)*. IEEE, 1–4. https://doi.org/10.1109/SECONW.2018.8396344

[38] Mohab A. Mangoud, Marios Lestas, and Taqwa Saeed. 2018. Molecular motors MIMO communications for nanonetworks applications. In *IEEE Wireless Communications and Networking Conference, WCNC*, Vol. 2018-April. IEEE, 1–5. https://doi.org/10.1109/WCNC.2018.8377406

[39] Daniel Tunc McGuiness, Stamatios Giannoukos, Alan Marshall, and Stephen Taylor. 2018. Parameter Analysis in Macro-Scale Molecular Communications Using Advection-Diffusion. *IEEE Access* 6 (2018), 46706–46717. https://doi.org/10.1109/ACCESS.2018.2866679

[40] James S. McLean. 1996. A re-examination of the fundamental limits on the radiation q of electrically small antennas. *IEEE Transactions on Antennas and Propagation* 44, 5 (may 1996), 672–676. https://doi.org/10.1109/8.496253

[41] Mark Mimee, Phillip Nadeau, Alison Hayward, Sean Carim, Sarah Flanagan, Logan Jerger, Joy Collins, Shane McDonnell, Richard Swartwout, Robert J Citorik, and Others. 2018. An ingestible bacterial-electronic system to monitor gastrointestinal health. *Science* 360, 6391 (2018), 915–918.

[42] Reza Mosayebi, Hamidreza Arjmandi, Amin Gohari, Masoumeh Nasiri-Kenari, and Urbashi Mitra. 2014. Receivers for diffusion-based molecular communication: Exploiting memory and sampling rate. *IEEE Journal on Selected Areas in Communications* 32, 12 (dec 2014), 2368–2380. https://doi.org/10.1109/JSAC.2014.2367732 arXiv:1405.0147

[43] Phillip Nadeau, Mark Mimee, Sean Carim, Timothy K Lu, and Anantha P Chandrakasan. 2017. 21.1 Nanowatt circuit interface to whole-cell bacterial sensors. In *Solid-State Circuits Conference (ISSCC), 2017 IEEE International*. IEEE, 352–353.

[44] Adam Noel, Karen C. Cheung, and Robert Schober. 2014. Improving receiver performance of diffusive molecular communication with Enzymes. *IEEE Transactions on Nanobioscience* 13, 1 (mar 2014), 31–43. https://doi.org/10.1109/TNB.2013.2295546 arXiv:1305.1926

[45] Adam Noel, Karen C. Cheung, and Robert Schober. 2014. Optimal receiver design for diffusive molecular communication with flow and additive noise. *IEEE Transactions on Nanobioscience* 13, 3 (sep 2014), 350–362. https://doi.org/10.1109/TNB.2014.2337239 arXiv:1308.0109

[46] Adam Noel, Karen C. Cheung, and Robert Schober. 2015. Joint Channel Parameter Estimation via Diffusive Molecular Communication. *IEEE Trans. Mol. Biol. Multi-Scale Commun.* 1, 1 (mar 2015), 4–17. https://doi.org/10.1109/TMBMC.2015.2465511 arXiv:1410.4252

[47] Adam Noel, Yansha Deng, Dimitrios Makrakis, and Abdelhakim Hafid. 2016. Active versus passive: Receiver model transforms for diffusive molecular communication. In *2016 IEEE Global Communications Conference, GLOBECOM 2016 - Proceedings*. https://doi.org/10.1109/GLOCOM.2016.7841566

[48] Mustafa Ozmen, Eamonn Kennedy, Jacob Rose, Pratistha Shakya, Jacob K Rosenstein, and Christopher Rose. 2018. High speed chemical vapor communication using photoionization detectors in turbulent flow. *IEEE Transactions on Molecular, Biological and Multi-Scale Communications* 4, 3 (2018), 160–170.

[49] Massimiliano Pierobon and Ian F Akyildiz. 2012. Capacity of a diffusion-based molecular communication system with channel memory and molecular noise. *IEEE Transactions on Information Theory* 59, 2 (2012), 942–954.

[50] Padarthi Naga Prasanth, Kakani Pruthvi Sumanth, Vijay K Chakka, and Gouriprasanna Roy. 2018. Experimental Implementation of Molecular Communication System using Sampling based Adaptive Threshold Variation Demodulation Algorithm. In *2018 IEEE International Conference on Advanced Networks and Telecommunications Systems (ANTS)*. IEEE, 1–5. https://doi.org/10.1109/ANTS.2018.8710039

[51] Yashar Rajavi, Mazhareddin Taghivand, Kamal Aggarwal, Andrew Ma, and Ada S Y Poon. 2017. An RF-powered FDD radio for neural microimplants. *IEEE Journal of Solid-State Circuits* 52, 5 (2017), 1221–1229.

[52] Giordano Rampioni, Livia Leoni, and Pasquale Stano. 2018. Molecular Communications in the Context of "Synthetic Cells" Research. *IEEE transactions on nanobioscience* (2018).

[53] Shirin Salehi, Naghmeh S. Moayedian, Shaghayegh Haghjooy Javanmard, and Eduard Alarcón. 2018. Lifetime improvement of a multiple transmitter local drug delivery system based on diffusive molecular communication. *IEEE Transactions on Nanobioscience* 17, 3 (2018), 352–360. https://doi.org/10.1109/TNB.2018.2850054

[54] Ehsan Samiei, Maryam Tabrizian, and Mina Hoorfar. 2016. A review of digital microfluidics as portable platforms for lab-on a-chip applications. *Lab on a Chip* 16, 13 (2016), 2376–2396.

[55] Huanhuan Shi, Kaixuan Nie, Bo Dong, Mengqiu Long, Hui Xu, and Zhengchun Liu. 2018. Recent Progress of Microfluidic Reactors for Biomedical Applications. *Chemical Engineering Journal* (2018).

[56] Daniel F. Sievenpiper, David C. Dawson, Minu M. Jacob, Tumay Kanar, Sanghoon Kim, Jiang Long, and Ryan G. Quarfoth. 2012. Experimental validation of performance limits and design guidelines for small antennas. *IEEE Transactions on Antennas and Propagation* 60, 1 (jan 2012), 8–19. https://doi.org/10.1109/TAP.2011.2167938

[57] Shimyn Slomovic, Keith Pardee, and James J Collins. 2015. Synthetic biology devices for in vitro and in vivo diagnostics. *Proceedings of the National Academy of Sciences* 112, 47 (2015), 14429–14435.

[58] Meric Turan, Bayram Cevdet Akdeniz, Mehmet Sukru Kuran, H. Birkan Yilmaz, Ilker Demirkol, Ali E. Pusane, and Tuna Tugcu. 2018. Transmitter Localization in Vessel-like Diffusive Channels using Ring-shaped Molecular Receivers. , 1 pages. https://doi.org/10.1109/LCOMM.2018.2871456

[59] Meriç Turan, MS Mehmet Şükrü Kuran, HB Birkan Yilmaz, Ilker Demirkol, and Tuna Tugcu. 2018. Channel Model of Molecular Communication via Diffusion in a Vessel-like Environment Considering a Partially Covering Receiver. *arxiv.org* (feb 2018). https://doi.org/10.1109/BlackSeaCom.2018.8433703 arXiv:1802.01180

[60] Harald Unterweger, Jens Kirchner, Wayan Wicket, Arman Ahmadzadeh, Doaa Ahmed, Vahid Jamali, Christoph Alexiou, Georg Fischer, and Robert Schober. 2018. Experimental Molecular Communication Testbed Based on Magnetic Nanoparticles in Duct Flow. In *IEEE Workshop on Signal Processing Advances in Wireless Communications, SPAWC*, Vol. 2018-June. https://doi.org/10.1109/SPAWC.2018.8446011 arXiv:1803.06990

[61] Alexander Van Reenen, Arthur M de Jong, Jaap M J den Toonder, and Menno W J Prins. 2014. Integrated lab-on-chip biosensing systems based on magnetic particle actuation–a comprehensive review. *Lab on a Chip* 14, 12 (2014), 1966–1986.

[62] Neeraj Varshney, Werner Haselmayr, and Weisi Guo. 2018. On Flow-Induced Diffusive Mobile Molecular Communication: First Hitting Time and Performance Analysis. (jun 2018). arXiv:1806.04784 http://arxiv.org/abs/1806.04784

[63] Wayan Wicke, Arman Ahmadzadeh, Vahid Jamali, Robert Schober, Harald Unterweger, and Christoph Alexiou. 2018. Molecular communication using magnetic nanoparticles. In *2018 IEEE Wireless Communications and Networking Conference (WCNC)*. IEEE, 1–6. https://doi.org/10.1109/WCNC.2018.8376970

[64] Wayan Wicke, Arman Ahmadzadeh, Vahid Jamali, Harald Unterweger, Christoph Alexiou, and Robert Schober. 2018. Magnetic Nanoparticle Based Molecular Communication in Microfluidic Environments. (aug 2018). arXiv:1808.05147 http://arxiv.org/abs/1808.05147

[65] Wayan Wicke, Tobias Schwering, Arman Ahmadzadeh, Vahid Jamali, Adam Noel, and Robert Schober. 2017. Modeling Duct Flow for Molecular Communication. (nov 2017). arXiv:1711.01479 http://arxiv.org/abs/1711.01479

[66] Tomohiro Yamada, Takumi Uezono, Kenichi Okada, Kazuya Masu, Akio Oki, and Yasuhiro Horiie. 2005. RF attenuation characteristics for in vivo wireless healthcare chip. *Japanese Journal of Applied Physics, Part 1: Regular Papers and Short Notes and Review Papers* 44, 7 A (jul 2005), 5275–5277. https://doi.org/10.1143/JJAP.44.5275

[67] Haoyang Zhai, Tadashi Nakano, A.V. Vasilakos, Kun Yang, and Qiang Liu. 2017. Increase detection algorithm for concentration-encoded diffusion-based molecular communication. In *Proceedings of the 4th ACM International Conference on Nanoscale Computing and Communication, NanoCom 2017*. ACM Press, New York, New York, USA, 1–6. https://doi.org/10.1145/3109453.3109465

[68] Mohammad Zoofaghari and Hamidreza Arjmandi. 2018. Diffusive Molecular Communication in Biological Cylindrical Environment. (jul 2018). arXiv:1807.02683 http://arxiv.org/abs/1807.02683